Available online at www.sciencedirect.com
SCIENCE DIRECT®
International Journal of Thermal Sciences 43 (2004) 575–586
International Journal of Thermal Sciences
www.elsevier.com/locate/ijts

Application to natural convection enclosed flows of a lattice Boltzmann BGK model coupled with a general purpose thermal boundary condition

Annunziata D'Orazio [a,*,1], Massimo Corcione [b], Gian Piero Celata [c]

[a] *Dipartimento di Meccanica e Aeronautica, Universita' di Roma "La Sapienza", Via Eudossiana 18, 00184 Roma, Italy*
[b] *Dipartimento di Fisica Tecnica, Universita' di Roma "La Sapienza", Via Eudossiana 18, 00184 Roma, Italy*
[c] *Istituto di Termofluidodinamica, ENEA, Via Anguillarese 301, 00060, S.M. Galeria, Roma, Italy*

Received 15 July 2003; accepted 21 November 2003

Available online 27 February 2004

Abstract

A thermal lattice BGK model with doubled populations, together with a new boundary condition for temperature and heat flux, is proposed to simulate the two-dimensional natural convection flow in a cavity. Numerical results for the problem of insulated horizontal walls and vertical walls at different temperatures are presented; they are found to be in good agreement with those of previous works. In addition, the problem of insulated horizontal walls and vertical walls heated and cooled by means of an imposed heat flux is discussed. Numerical results are presented as compared with theoretical values and they are found to be in satisfactory agreement. Therefore, the method can capture fundamental behaviors in thermal flows of engineering interest.

Keywords: Lattice Boltzmann thermal model; Doubled populations BGK; Dirichlet/Neumann thermal boundary conditions; Natural convection; Enclosures

1. Introduction

In the last decade lattice kinetic theory, and most notably the lattice Boltzmann method (LBM) (see, for example, Higuera et al. [1], Benzi et al. [2], Alexander et al. [3], Chen and Doolen [4] and Succi [5]), have met with significant success for the numerical simulation of a large variety of fluid flows, including real-world engineering applications. The lattice Boltzmann equation (LBE) is a minimal form of the Boltzmann kinetic equation, which is the evolution equation for a continuous one-body distribution function $f(\vec{x}, \vec{v}, t)$, wherein all details of molecular motion are removed except those that are strictly needed to represent the hydrodynamic behaviour at the macroscopic scale. The result is a very elegant and simple evolution equation for a discrete distribution function, or discrete population $f_i(\vec{x}, t) = f(\vec{x}, \vec{c}_i, t)$, which describes the probability to find a particle at lattice position $\vec{x}$ at time t, moving with speed $\vec{c}_i$. In a hydrodynamic simulation by using the LBE, one solves the only-two-steps evolution equations of the distribution functions of fictitious fluid particles: they move synchronously along rectilinear trajectories on a lattice space and then relax towards the local equilibrium because of the collisions. With respect to the more conventional numerical methods commonly used for the study of fluid flow situations, the kinetic nature of LBM introduces several advantages, including easy implementation of boundary conditions and fully parallel algorithms. In addition, the convection operator is linear, no Poisson equation for the pressure must be resolved and the translation of the microscopic distribution function into the macroscopic quantities consists of simple arithmetic calculations.

However, whereas LBE techniques shine for the simulation of isothermal, quasi-incompressible flows in complex geometries, and LBM has been shown to be useful in applications involving interfacial dynamics and complex boundaries (see, for example, the recent works of Nie et al. [6], Lim et al. [7], Nguyen et al. [8], Hoekstra et al. [9], Facin et al. [10], Inamuro et al. [11] and Dupuis et al. [12]), the application to fluid flow coupled with non negligible heat

* Corresponding author.
E-mail addresses: annunziata.dorazio@casaccia.enea.it (A. D'Orazio), massimo.corcione@uniroma1.it (M. Corcione), celata@casaccia.enea.it (G.P. Celata).

[1] I would like to thank Sauro Succi for his valuable discussions and suggestions about Lattice Boltzmann Methods. Thanks to "Istituto delle Applicazioni del Calcolo" (IAC-CNR) for kind hospitality during the development of this work.

1290-0729/$ – see front matter
doi:10.1016/j.ijthermalsci.2003.11.002

Nomenclature

$\vec{c}_i$	$= (c_{ix}, c_{iy})$ discrete particle speeds
c	$= \mathrm{d}x/\mathrm{d}t$ minimum speed on the lattice
c_s	lattice sound speed
$\mathrm{d}t$	time increment
$\mathrm{d}x$	$= \mathrm{d}y$ lattice spacing
ΔT	$= T_h - T_c$ temperature difference between hot and cold wall
e	internal energy density
e'	counter-slip internal energy density used in the thermal boundary conditions
f, g	continuous single-particle distribution functions for density-momentum and internal energy-heat flux fields
$\tilde{f}, \tilde{g}$	modified continuous single-particle distribution functions for density-momentum and internal energy-heat flux fields
f_i, g_i	discrete distribution functions
$\tilde{f}_i, \tilde{g}_i$	modified discrete distribution functions
f_i^e, g_i^e	equilibrium discrete distribution functions
G_1	$= \beta g(T - \overline{T})$ buoyancy force per unit mass
G_2	$= \beta g(T - T_O)$ buoyancy force per unit mass
$\vec{g}$	$= (-g, 0)$ acceleration due to the gravity
H, L	cavity height, width
k	thermal conductivity
Nu_1	$= -\frac{H}{\Delta T}\frac{\partial T}{\partial y}\|_{\text{wall}}$ Nusselt number
Nu_2	$= -\frac{H}{\Delta T}\frac{q_y}{k}$ Nusselt number
$\overline{Nu}$	$= \frac{1}{H}\int_0^H Nu\,\mathrm{d}x$ average Nusselt number
Pr	$= \nu/\chi$ Prandtl number
$\vec{q}$	$= (q_x, q_y)$ heat flux
R	constant of the gas
Ra_1	$= \beta g \Delta T H^3/\nu\chi$ Rayleigh number
Ra_2	$= \beta g \Delta T H^4 q_y Pr/\nu^2 k$ Rayleigh number
t	temporal coordinate
$T, \overline{T}$	local, average temperatures
T_O	temperature at the cavity centre
T^{**}	$= \chi\nu Ra_2^{4/5}/\beta g H^3$ reference temperature
$\vec{x}$	$= (x, y)$ spatial coordinate
y^{**}	$= H\,Ra_2^{-1/5}$ reference horizontal coordinate
$\vec{u}$	$= (u, v)$ flow velocity
$\vec{u}'$	$= \vec{\xi} - \vec{u}$ peculiar speed of the molecules
(U, V)	flow velocity at wall
V^*	$= \nu/Pr\,H$ diffusion, reference velocity
V^{**}	$= \chi\,Ra_2^{2/5}/H$ reference velocity
Z	continuous viscous heating term
Z_i	discrete viscous heating term
w_i	weights of discrete populations

Greek symbols

β	coefficient of thermal expansion
ν	kinematic diffusivity
χ	thermal diffusivity
$\rho, \bar{\rho}$	local, average fluid density
$\vec{\xi}$	absolute velocity of molecules
τ_f, τ_g	relaxation times towards the local equilibrium

Super- and sub-scripts

e	equilibrium
h, c	hot, cold
W, N, E, S	west, north, east, south

transfer turned out to be much more difficult (see, for example, Chen et al. [13] and [14], Mc Namara et al. [15], Chen [16], Vahala et al. [17], Karlin et al. [18], Luo [19], Succi et al. [20] and Lallemand and Luo [21]).

The LBE thermal models fall into three categories: the multi-speed approach, the passive scalar approach and the doubled populations approach. The so-called multi-speed approach, which is a straightforward extension of the LBE isothermal models, makes theoretically possible to express both heat flux and temperature in terms of higher-order kinetic moments of the particle distribution functions $f_i(\vec{x}, t)$. It implies that higher-order velocity terms are involved in the formulation of equilibrium distribution and additional speeds are required by the corresponding lattices. The latter is arguably the major source of numerical instabilities of thermal lattice kinetic equations; in addition, it can seriously impair the implementation of the boundary conditions, a vital issue for the practical applications.

The passive scalar and the doubled populations approaches are based on the idea of dispensing with the explicit representation of heat flux in terms of kinetic moments of the particle distribution function $f(\vec{x}, \vec{v}, t)$.

A successful strategy consists of solving the temperature equation independently of LBE, possibly even with totally different numerical techniques. If the viscous heat dissipation and compression work done by the pressure are negligible, the temperature evolution equation is the same of a passive scalar, and this approach enhances the numerical stability (see, for example, Vahala et al. [17]); the coupling to LBE is made by expressing the fluid pressure as the gradient of an external potential. Clearly, this strategy represents a drastic departure from a fully kinetic approach, and lacks some elegance.

A more elegant possibility is to double the degrees of freedom and express thermal energy density and heat flux still as kinetic moments of a separate 'thermal' distribution $g(\vec{x}, \vec{v}, t)$ (see He et al. [22]). The advantage of this latter approach is that no kinetic moment beyond the first order is ever needed, since heat flux (third order vector moment of f) is simply expressed as the first order vector moment of g: as a result, disruptive instabilities conventionally attributed to

the failure of reproducing higher-order moments in a discrete lattice are potentially avoided/mitigated. With respect to the previous approaches, the method is able to include viscous heating effects, and the boundary conditions are easily implemented because both f and g live in the same lattice, where additional speeds are not necessary.

As far as the thermal boundary conditions are concerned, LBE techniques usually handle the Dirichlet-type constraints; in contrast, the Neumann-type constraints are either limited to insulated walls or obtained imposing the temperature gradient at the wall through a strategy of transfer to a Dirichlet-type condition.

For a wide class of real phenomena, the fixed temperature condition is clearly inadequate. Examples are represented by the cooling of devices, where the problem is characterized by an imposed thermal power to be removed, or by the air behavior in building rooms, where the temperature of the external walls is a direct consequence of the heat flux administered to the walls.

In this framework, main aim of the present paper is to propose, discuss and validate a general purpose thermal boundary condition (GPTBC). The GPTBC proposed here, successfully demonstrated for the Dirichlet-type constraint in the case of thermal Couette and Poiseuille flows (see D'Orazio and Succi [23] and D'Orazio et al. [24]), can simulate explicitly either imposed wall temperature (Dirichlet-type constraint) or imposed wall heat fluxes (Neumann-type constraint), which allows LBM to be used for successful simulation of many types of heat transfer and fluid flows applications. Thus, the method can become an effective and alternative easy-to-apply tool, as well as the athermal LBE counterpart, especially for all those situations wherein the use of the usual theoretical approaches may fail, e.g., due to the complexity of the geometry. The validity of the developed GPTBC is demonstrated through its application to different cases of natural convection in enclosed spaces, which today represents an active subfield in heat transfer research.

The large number of papers available in the open literature, to which the reader is referred, testifies the great interest of this topic (see, for example, Janssen et al. [25], Xin and Le Quere [26], Versteegh and Nieuwstadt [27], Dol and Hanjalic [28], Wang et al. [29] and Corcione [30]).

This great interest is due to the several fields in which natural convection is involved and to its importance in many engineering applications, e.g., heat transfer in buildings, solar energy collection, heat removal in micro electronics, cooling of nuclear reactors, dispersion of fire fumes in buildings and tunnels, ventilation of rooms. Compared with this great applicative interest, natural convection research is characterized by several theoretical and practical issues. The buoyancy-induced heat and momentum transfer in enclosures, also in simple geometries, strongly depends on geometric and physical conditions. Several regimes and complex phenomena of successive transitions can take place. Standard simulation techniques CFD cannot predict the behaviour of natural convection systems with high geometric complexity, or where viscous heating effects and/or non-trivial conditions, related to the rheological law, are non-negligible. As said, alternative approaches can be useful and required. The present paper deals with the application of the thermal LBM to the natural convection flow in a square cavity with differently heated vertical walls, and with a uniform heat flux heating and cooling both vertical walls.

2. The thermal LBE model

This paper will deal with the double-populations LBE model proposed by He et al. [22]. The main idea is to view a thermal flow as a mixture of material particles and thermal excitations (*fluons* and *phonons* for brevity) described by two separate distribution functions f and g. Fluons carry mass and momentum according to the standard kinetic moments:

$$\rho(\vec{x},t) = \int f(\vec{x},\vec{\xi},t)\,\mathrm{d}\vec{\xi} \tag{1}$$

$$\rho(\vec{x},t)\vec{u}(\vec{x},t) = \int \vec{\xi}\, f(\vec{x},\vec{\xi},t)\,\mathrm{d}\vec{\xi} \tag{2}$$

whereas phonons are in charge of the thermal energy density and the corresponding heat flux:

$$\rho e(\vec{x},t) = \int g(\vec{x},\vec{\xi},t)\,\mathrm{d}\vec{\xi} \tag{3}$$

$$\vec{q}(\vec{x},t) = \int \vec{v}' g(\vec{x},\vec{\xi},t)\,\mathrm{d}\vec{\xi} \tag{4}$$

where ρ is the fluid density, $\vec{u}$ is the flow speed and $\vec{\xi}$ is the absolute velocity of the molecules; in addition, $\vec{v}' = \vec{\xi} - \vec{u}$ is the molecular peculiar speed relative to the flow speed. Of course, in a real gas where mass, momentum and energy are carried by the same physical molecules, the following relationship must hold:

$$g(\vec{x},\vec{\xi},t) = \frac{|\vec{v}'|^2}{2} f(\vec{x},\vec{\xi},t) \tag{5}$$

Therefore, the evolution equation for g is entirely specified by the corresponding Boltzmann equation for f. More specifically:

$$\partial_t f + (\vec{\xi}\cdot\nabla) f = \Omega(f) \tag{6}$$

$$\partial_t g + (\vec{\xi}\cdot\nabla) g = 0.5|\vec{v}'|^2 \Omega(f) - f(\vec{\xi}-\vec{u})\cdot\left[\partial_t\vec{u} + (\vec{\xi}\cdot\nabla)\vec{u}\right] \tag{7}$$

where $\Omega(f)$ is the collision operator and the last term in Eq. (7),

$$-f(\vec{\xi}-\vec{u})\cdot\left[\partial_t\vec{u} + (\vec{\xi}\cdot\nabla)\vec{u}\right] = -fZ \tag{8}$$

represents the viscous heating.

The simplest and by now most popular form of lattice Boltzmann equation is the lattice BGK, for Bhatnagar, Gross and Krook (see Qian et al. [31]). The collision operator is

expressed as a single relaxation time to the local equilibrium so that

$$\Omega(f) = -\frac{f - f^e}{\tau_f} \tag{9}$$

$$0.5\left|\vec{v}'\right|^2 \Omega(f) = \Omega(g) = -\frac{g - g^e}{\tau_g} \tag{10}$$

The Lattice Boltzmann Model is obtained by a discretization of the velocity space: the *discrete* one-body distribution function is assumed to move along the lattice link $\mathrm{d}\vec{x}_i = \vec{c}_i\,\mathrm{d}t$, connecting nearest neighbours, and to change its value because of the collisions, while integrals over all velocity space can be replaced by sums over the finite set of speed, in order to calculate macroscopic variables at the lattice sites. For all details about the appropriate discretization of the microscopic velocity space, in order to recover the continuity and momentum equations at the Navier–Stokes level, by means of a Gaussian–Hermite quadrature, the reader is referred to the important results of He and Luo [32]. Details about the derivation of the discrete scheme for the thermal energy evolution equation, by means of an analogous Gaussian–Hermite quadrature, can be found in He et al. [22]. Precisely along this line of thought, and in order to guarantee that the kinematic viscosity, ν, has the same expression in both Navier–Stokes and energy equations, when a Chapman–Enskog expansion has been performed, a second order strategy to integrate Eqs. (6), (9) and (7), (10) is adopted by He et al. [22]. In order to avoid the implicitness of the scheme, they introduce new discrete distribution functions $\tilde{f}_i$ and $\tilde{g}_i$

$$\begin{aligned}\tilde{f}_i &= f_i + \frac{0.5\,\mathrm{d}t}{\tau_f}\left(f_i - f_i^e\right)\\ \tilde{g}_i &= g_i + \frac{0.5\,\mathrm{d}t}{\tau_g}\left(g_i - g_i^e\right) + \frac{\mathrm{d}t}{2} Z_i f_i\end{aligned} \tag{11}$$

where f_i and g_i are the discrete populations which evolve when a standard first order integration strategy is adopted.

The term $Z_i = (\vec{c}_i - \vec{u}) \cdot D_i \vec{u}$ represents the effects of viscous heating and $D_i = \partial_t + \vec{c}_i \cdot \nabla$ is the material derivative along direction $\vec{c}_i$. More specifically, it can be expressed as:

$$\begin{aligned}Z_i = &\left[\vec{c}_i - \vec{u}(\vec{x}, t)\right]\\ &\cdot \left[\vec{u}(\vec{x} + \vec{c}_i\,\mathrm{d}t, t + \mathrm{d}t) - \vec{u}(\vec{x}, t)\right]/\mathrm{d}t\end{aligned} \tag{12}$$

This new distribution functions obey thus a set of lattice BGK equations in the form:

$$\begin{aligned}&\tilde{f}_i(\vec{x} + \vec{c}_i\,\mathrm{d}t, t + \mathrm{d}t) - \tilde{f}_i(\vec{x}, t)\\ &\quad = -\frac{\mathrm{d}t}{\tau_f + 0.5\,\mathrm{d}t}\left(\tilde{f}_i - f_i^e\right)\end{aligned} \tag{13}$$

$$\begin{aligned}&\tilde{g}_i(\vec{x} + \vec{c}_i\,\mathrm{d}t, t + \mathrm{d}t) - \tilde{g}_i(\vec{x}, t)\\ &\quad = -\frac{\mathrm{d}t}{\tau_g + 0.5\,\mathrm{d}t}\left(\tilde{g}_i - g_i^e\right) - \frac{\mathrm{d}t\,\tau_g}{\tau_g + 0.5\,\mathrm{d}t} Z_i f_i\end{aligned} \tag{14}$$

where τ_f, τ_g are the relaxation times and f_i^e, g_i^e are the equilibrium distribution functions. In the sequel, the reader is referred to the two-dimensional square lattice with the nine speeds, represented in Fig. 1, which is sufficient to guarantee the recovering of the Navier–Stokes equations after a Chapman–Enskog expansion:

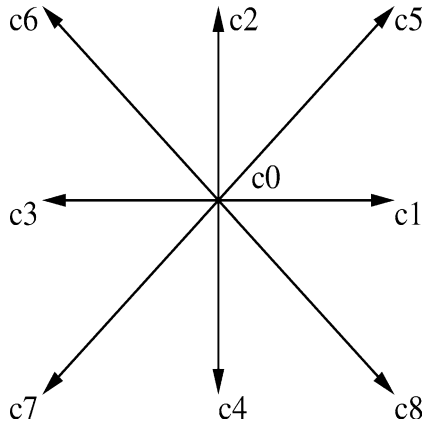

Fig. 1. Nine-speed square lattice.

$$\begin{aligned}&\vec{c}_i = \left(\cos\left(\frac{i-1}{4}\pi\right), \sin\left(\frac{i-1}{4}\pi\right)\right)c\\ &\quad i = 1, \ldots, 8 \quad \vec{c}_0 = 0\end{aligned} \tag{15}$$

where $c^2 = 3RT$ and T is the temperature. The equilibrium density distributions are chosen in the form of a quadratic expansion of a Maxwellian as follows:

$$f_i^e = w_i \rho\left[1 + \frac{3\vec{c}_i \cdot \vec{u}}{c^2} + \frac{9(\vec{c}_i \cdot \vec{u})^2}{2c^4} - \frac{3(u^2 + v^2)}{2c^2}\right] \tag{16}$$

$$g_0^e = -w_0 \frac{3\rho e}{2}\frac{(u^2 + v^2)}{c^2} \tag{17}$$

$$\begin{aligned}g^e_{\rightarrow,\uparrow,\leftarrow,\downarrow} = w_1 \rho e\Bigg[&1.5 + \frac{1.5\vec{c}_i \cdot \vec{u}}{c^2} + \frac{4.5(\vec{c}_i \cdot \vec{u})^2}{c^4}\\ &- \frac{1.5(u^2 + v^2)}{c^2}\Bigg]\end{aligned} \tag{18}$$

$$\begin{aligned}g^e_{\nearrow,\nwarrow,\swarrow,\searrow} = w_2 \rho e\Bigg[&3 + \frac{6\vec{c}_i \cdot \vec{u}}{c^2} + \frac{4.5(\vec{c}_i \cdot \vec{u})^2}{c^4}\\ &- \frac{1.5(u^2 + v^2)}{c^2}\Bigg]\end{aligned} \tag{19}$$

In the above, $\vec{u} \equiv (u, v)$, $\rho e = \rho RT$ (in $2D$), the weights of the different populations are

$$\begin{aligned}&w_0 = \frac{4}{9}, \qquad w_1 = \frac{1}{9}, \quad i = \rightarrow, \uparrow, \leftarrow, \downarrow\\ &w_2 = \frac{1}{36}, \quad i = \nearrow, \nwarrow, \swarrow, \searrow\end{aligned} \tag{20}$$

and the arrows denote the corresponding discrete speeds. The terms enclosed by the square bracket, multiplied by the corresponding weights w_i, will be called *corresponding form for equilibrium*.

Finally, the hydrodynamic variables, density and momentum, can be calculated as (discrete) kinetic moments of $\tilde{f}_i$ of zeroth and first order, respectively, whereas zeroth and first

order kinetic moments of $\tilde{g}_i$ are used to express thermal energy density and corresponding heat flux. Therefore, from the originate equations

$$\rho = \sum_i f_i, \qquad \rho e = \sum_i g_i$$
$$\rho\vec{u} = \sum_i \vec{c}_i f_i, \qquad \vec{q} = \sum_i (\vec{c}_i - \vec{u}) g_i \tag{21}$$

by using Eqs. (11), and reminding that

$$\sum_i g_i^e = \rho e, \qquad \sum_i \vec{c}_i g_i^e = \rho e \vec{u} \tag{22}$$

we can write

$$\rho = \sum_i \tilde{f}_i, \qquad \rho e = \sum_i \tilde{g}_i - \frac{\mathrm{d}t}{2} \sum_i f_i Z_i \tag{23}$$
$$\rho\vec{u} = \sum_i \vec{c}_i \tilde{f}_i$$
$$\vec{q} = \left(\sum_i \vec{c}_i \tilde{g}_i - \rho e \vec{u} - \frac{\mathrm{d}t}{2} \sum_i \vec{c}_i f_i Z_i \right) \frac{\tau_g}{\tau_g + 0.5\,\mathrm{d}t} \tag{24}$$

The coupling between the two populations occurs at two levels:

(i) The local equilibrium f_i^e depends on the actual internal energy density e.
(ii) The phonon distribution is forced by the viscous heating term $Z_i f_i$.

Constraint (i) is the expression of thermodynamic consistency, whereas (ii) specifically relates to viscous heating effects. To improve the numerical stability, space–time independent *average* values of T are used to calculate the lattice speed in the local equilibria of $\tilde{f}$ and $\tilde{g}$ (average thermohydrodynamic consistency), as made in the original paper:

$$c^2 = 3R\overline{T} \tag{25}$$

where $\overline{T}$ is the average temperature. The kinematic viscosity and the thermal diffusivity are given by:

$$\nu = \tau_f R\overline{T}, \qquad \chi = 2\tau_g R\overline{T} \tag{26}$$

In the sequel, as usual in lattice Boltzmann methods, all the variables are normalized from the reference velocity $(3R\overline{T})^{0.5}$ and the reference length $\mathrm{d}x$.

3. Natural convection in a square cavity: A test-case for Dirichlet thermal boundary condition

In order to demonstrate the validity of the present GPTBC in case of imposed wall temperature, as described in next Section 3.1, a two-dimensional flow in a square cavity is considered. The four walls of the cavity are at rest, so that the wall speed is $(U, V) = (0, 0)$. The horizontal (West and East) walls are insulated and the vertical walls (North and South) are maintained at constant but different temperatures

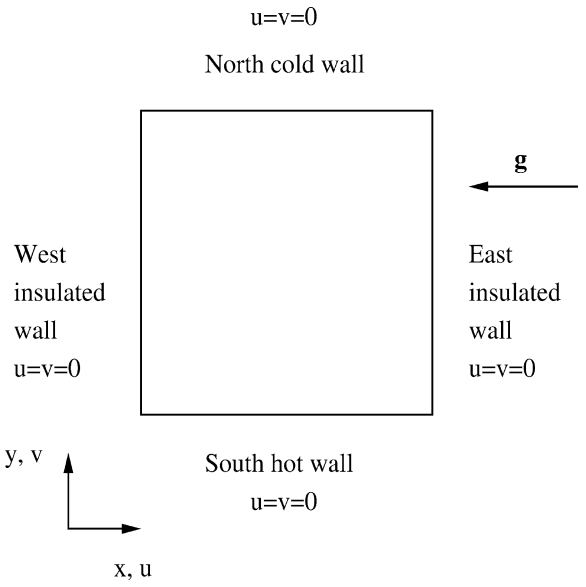

Fig. 2. Imposed temperature flow configuration.

T_h and T_c (see Fig. 2). With the Boussinesq approximation, all the fluid properties are considered as constant, except in the body force term in the Navier–Stokes equations, where the fluid density is assumed $\rho = \bar{\rho}[1 - \beta(T - \overline{T})]$; β is the thermal expansion coefficient, $\bar{\rho}$, $\overline{T}$ are the average fluid density and temperature and $\vec{g} = -g\vec{i}$ is the gravitational acceleration vector.

The major control parameter is the Rayleigh number $Ra_1 = \beta g \Delta T H^3 Pr/\nu^2$, where ΔT is the temperature difference between the hot and cold walls; $Pr = \nu/\chi$ is the Prandtl number, measuring the momentum to heat diffusivity ratio, and H is the height or width of the cavity.

For laminar convection in this flow configuration, in which the viscous heating is assumed to be negligible, the reader is referred to the benchmark solutions given by Hortmann et al. in [33], by De Vahl Davis in [34] and by Barakos et al. in [35].

The most common set-up to simulate nearly incompressible flow consists of driving the flow by means of a force per unit mass $G_1 = \beta g(T - \overline{T})$, representing the buoyancy effect. More specifically,

$$\tilde{f}_i(\vec{x} + \vec{c}_i\,\mathrm{d}t, t + \mathrm{d}t) - \tilde{f}_i(\vec{x}, t) = -\frac{\mathrm{d}t}{\tau_f + 0.5\,\mathrm{d}t}\left(\tilde{f}_i - f_i^e\right) + \frac{\mathrm{d}t\,\tau_f}{\tau_f + 0.5\,\mathrm{d}t} \frac{3G_1(c_{ix} - u)}{c^2} f_i^e \tag{27}$$

$$\sum_i \tilde{f}_i = \rho, \qquad \sum_i \tilde{f}_i c_{ix} = \rho u - \frac{\mathrm{d}t}{2} F_b$$
$$\sum_i \tilde{f}_i c_{iy} = \rho v \tag{28}$$

where $F_b = \rho G_1$.

3.1. Boundary conditions

With regard to the velocity field, the non-slip boundary conditions are applied to the four walls of the cavity. These are obtained by means of the non-equilibrium bounce back rule, which we describe in appendix, proposed by Zou and He [36].

With regard to the thermal field, a thermal counter-slip approach is used here. The counter-slip idea has been proposed for the velocity boundary conditions by Inamuro et al. [37], who suggested also possible application even to thermal models with imposed wall temperature (Dirichlet-type constraint). Imposed wall temperature and zero heat flux boundary conditions by means of the counter-slip approach, which has been applied for the first time by D'Orazio and Succi [23] and D'Orazio et al. [24] in case of thermal Couette and Poiseuille flows, are described here.

The incoming unknown thermal populations are assumed to be equilibrium distribution functions with a counter-slip thermal energy density e', which is determined so that suitable constraints are verified. if the North wall is considered, where $T = T_N$, the unknown $\tilde{g}_{\downarrow}$, $\tilde{g}_{\searrow}$ and $\tilde{g}_{\swarrow}$ are chosen

$$\tilde{g}_i = \rho(e_N + e')[\text{corresponding form for equilibrium}] \quad i = \downarrow, \searrow, \swarrow \tag{29}$$

By definition:

$$\sum_i \tilde{g}_i = \rho e_N + \frac{\mathrm{d}t}{2} \sum_i f_i Z_i \tag{30}$$

which yields

$$\rho e_N + \rho e' = \frac{\rho e_N + \frac{\mathrm{d}t}{2} \sum_i f_i Z_i - K}{\frac{1}{3} - \frac{1}{2}\frac{V}{c} + \frac{1}{2}\frac{V^2}{c^2}} \tag{31}$$

where K is the sum of the six known populations coming from nearest wall and fluid nodes, e_N denotes the imposed thermal energy density at the North wall, and the viscous heating term appears for generality. This boundary condition is found to provide significant stability and accuracy. Probably, this is due to the fact that, in order to find the unknown populations coming from the external nodes, the constraint (30) is applied to the complete set of known populations coming from the fluid field. He et al. [38] proved that the counter-slip boundary condition proposed by Inamuro et al. [37] for the velocity, and any other scheme which uses all fluid populations to generate the unknowns, yields a zero slip-velocity at the wall. It is assumed that the proof holds in this thermal case as well. At the insulated walls (the West wall as an example and still regarding the viscous heating for generality), the constraint on the heat flux is obtained by imposing $q_x = 0$ in the second equation of Eqs. (24), so that

$$\sum_i c_{ix} \tilde{g}_i = 0.5\,\mathrm{d}t \sum_i c_{ix} f_i Z_i + \rho e_W U \tag{32}$$

where e_W denotes the thermal energy density current value (coming from the run) at the West wall. The unknown populations $\tilde{g}_{\rightarrow}$, $\tilde{g}_{\nearrow}$ and $\tilde{g}_{\searrow}$, chosen as

$$\tilde{g}_i = \rho(e_W + e')[\text{corresponding form for equilibrium}] \quad i = \rightarrow, \nearrow, \searrow \tag{33}$$

become

$$\tilde{g}_{\rightarrow,\nearrow,\searrow} = \left[\frac{1}{\frac{1}{3} + 0.5\frac{U}{c} + 0.5\frac{U^2}{c^2}}\right] \times \left[\left(\sum_{\leftarrow,\nwarrow,\swarrow} \tilde{g}_i\right) + \frac{\mathrm{d}t}{2} \sum_W \frac{c_i}{c} Z_i f_i + \rho e_W \frac{U}{c}\right] \times [\text{corresponding form for equilibrium}] \tag{34}$$

The corners nodes are treated in a similar way and the counter-slip procedure can be applied to the five unknown incoming populations at the corner. As an example, at the North–West corner the unknown populations are $\tilde{g}_{\rightarrow}$, $\tilde{g}_{\downarrow}$, $\tilde{g}_{\searrow}$, $\tilde{g}_{\nearrow}$ and $\tilde{g}_{\swarrow}$; if the corner node is a fixed temperature wall node, it follows that

$$\rho e' = \frac{\rho e_N (5 - 4\frac{U}{c} - 5\frac{U^2}{c^2}) + 6\,\mathrm{d}t \sum_i f_i Z_i - 12K}{7 + 4\frac{U}{c} + 5\frac{U^2}{c^2}} \tag{35}$$

where K is the sum of the four known populations coming from nearest wall and fluid nodes, e_N is still the imposed value of the North wall thermal energy density, and viscous heating term appears for generality.

3.2. Numerical results

For a comparison with the benchmark solutions, results for the Rayleigh number ranging from 10^3 to 10^6, and the Prandtl number $Pr = 0.71$, are reported. The average temperature used in particle equilibria is $\overline{T} = (T_S + T_N)/2$ with $T_S = T_h = 20.0$ and $T_N = T_c = 1.0$; the relaxation times are chosen $\tau_f = 0.1$ and $\tau_g = 0.0704$. To simulate the flow for Rayleigh number $Ra_1 = 10^3$ and $Ra_1 = 10^4$, a 129×129 grid is used with the diffusion velocity $V^* = \nu/Pr\,H = 0.3667 \times 10^{-3}$. For $Ra_1 = 10^5$ and $Ra_1 = 10^6$, a 205×205 grid is used with the diffusion velocity $V^* = \nu/Pr\,H = 0.2301 \times 10^{-3}$. The local Nusselt number and the average value are calculated as

$$Nu_1 = -\frac{H}{\Delta T} \frac{\partial T}{\partial y}\Big|_{\text{wall}} \tag{36}$$

$$\overline{Nu}_1 = \frac{1}{L} \int_0^L Nu_1\,\mathrm{d}x \tag{37}$$

where the temperature gradient is obtained by means of a three points formula. Table 1 reports the maximum horizontal velocity $v_{\max}/V^*$ at $y/H = 0.5$, the maximum vertical velocity $u_{\max}/V^*$ at $x/L = 0.5$ and the locations where they occur. Table 2 reports the maximum and minimum values of the Nusselt number along the hot wall,

Table 1
Natural convection in a square cavity with vertical walls at different temperatures. Comparison of laminar solution with previous works for different Rayleigh number (Ra_1) and $Pr = 0.71$: maximum horizontal velocity v_{max}/V^* at $y/H = 0.5$, maximum vertical velocity u_{max}/V^* at $x/L = 0.5$, and, in parentheses, the locations where they occur

	u_{max} (y/H)	v_{max} (x/L)
	$Ra = 10^3$	
This work	3.7006 (0.1797)	3.6532 (0.8125)
Barakos et al.	4.1301 (0.181)	4.0768 (0.806)
De Vahl Davis	3.697 (0.178)	3.649 (0.813)
Fusegi, cited in [35]	3.4906 (0.200)	3.5172 (0.833)
Hortmann et al.	− (-)	− (-)
	$Ra = 10^4$	
This work	19.6803 (0.1172)	16.2370 (0.8203)
Barakos et al.	19.71719 (0.119)	16.262470 (0.818)
De Vahl Davis	19.617 (0.119)	16.178 (0.823)
Fusegi, cited in [35]	18.9588 (0.117)	16.9366 (0.817)
Hortmann et al.	19.6295 (0.1193)	16.1802 (0.8265)
	$Ra = 10^5$	
This work	68.7122 (0.0637)	34.8225 (0.8529)
Barakos et al.	68.7462 (0.066)	35.1725 (0.859)
De Vahl Davis	68.59 (0.066)	34.73 (0.855)
Fusegi, cited in [35]	65.8152 (0.065)	39.1694 (0.855)
Hortmann et al.	68.6396 (0.0657)	34.7399 (0.8558)
	$Ra = 10^6$	
This work	221.1869 (0.0392)	64.8679 (0.8529)
Barakos et al.	220.7651 (0.039)	64.8813 (0.859)
De Vahl Davis	219.36 (0.0379)	64.63 (0.850)
Fusegi, cited in [35]	218.2373 (0.033)	70.7796 (0.856)
Hortmann et al.	220.461 (0.0390)	64.8367 (0.8505)

the location where they occur and the average value $\overline{Nu}_1$. The relation between $\overline{Nu}_1$ and Ra_1 may be described as a power-law equation:

$$\overline{Nu}_1 = a(Ra_1)^b \tag{38}$$

where $a = 0.1425$ and $b = 0.2988$, which are in good agreement with the results $(a, b) = (0.142, 0.299)$ reported by Barakos et al. [35]. Fig. 3 shows the normalized temperature profiles $[T(y) - T_N]/\Delta T$ at the mid-width $x/L = 0.5$ of the cavity, for Rayleigh number ranging from 10^3 to 10^6 and $Pr = 0.71$.

For the same values of the Rayleigh and Prandtl numbers, Fig. 4 shows the normalized vertical velocity $u(y)/V^*$ at the mid-width $x/L = 0.5$ of the cavity, whereas Fig. 5 shows the normalized horizontal velocity $v(x)/V^*$ at the mid-height $y/H = 0.5$.

The transition from the motionless conduction dominated regime to the convection dominated regime, which takes place after $Ra = 10^3$, can be observed. The increase of the motion strength with increasing Rayleigh number, which brings to the formation of a quasi-motionless fluid core embedded between two boundary layer regions adjacent to the differently heated walls, for $Ra = 10^5 - Ra = 10^6$, is well captured.

Table 2
Natural convection in a square cavity with vertical walls at different temperatures. Comparison of laminar solution with previous works for different Rayleigh number (Ra_1) and $Pr = 0.71$: maximum, minimum and average values of the Nusselt number (Nu_1) at the hot-wall, and, in parentheses, the location where they occur

	$\overline{Nu}$	Nu_M (x/L)	Nu_m (x/L)
	$Ra = 10^3$		
This work	1.117	1.501 (0.086)	0.698 (0.953)
Barakos et al.	1.114	1.581 (0.099)	0.670 (0.994)
De Vahl Davis	1.118	1.505 (0.092)	0.692 (1.000)
Fusegi, cited in [35]	1.105	1.420 (0.083)	0.764 (1.000)
	$Ra = 10^4$		
This work	2.235	3.507 (0.148)	0.584 (0.984)
Barakos et al.	2.245	3.539 (0.143)	0.583 (0.994)
De Vahl Davis	2.243	3.528 (0.143)	0.586 (1.000)
Fusegi, cited in [35]	2.302	3.652 (0.623)	0.611 (1.000)
	$Ra = 10^5$		
This work	4.504	7.658 (0.088)	0.728 (0.990)
Barakos et al.	4.510	7.636 (0.085)	0.773 (0.999)
De Vahl Davis	4.519	7.717 (0.081)	0.729 (1.000)
Fusegi, cited in [35]	4.646	7.795 (0.083)	0.787 (1.000)
	$Ra = 10^6$		
This work	8.767	17.288 (0.0441)	0.998 (0.990)
Barakos et al.	8.806	17.442 (0.0368)	1.001 (0.999)
De Vahl Davis	8.800	17.925 (0.0378)	0.989 (1.000)
Fusegi, cited in [35]	9.012	17.670 (0.0379)	1.257 (1.000)

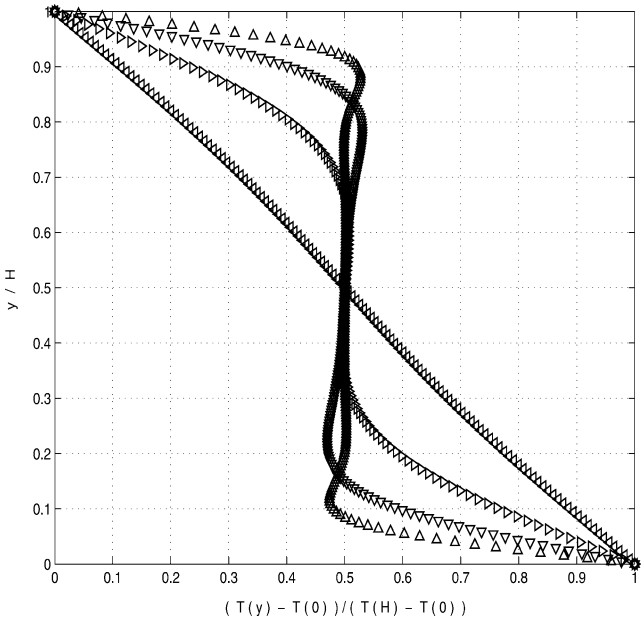

Fig. 3. Normalized temperature profiles at $x/L = 0.5$, $\Delta T = 19.0$, $Pr = 0.71$; ◁: $Ra = 10^3$, ▷: $Ra = 10^4$, ▽: $Ra = 10^5$, △: $Ra = 10^6$.

4. Natural convection in a square cavity: A test-case for Neumann thermal boundary condition

In order to validate the GPTBC in case of imposed non-zero wall heat flux, as described in next Section 4.1, a

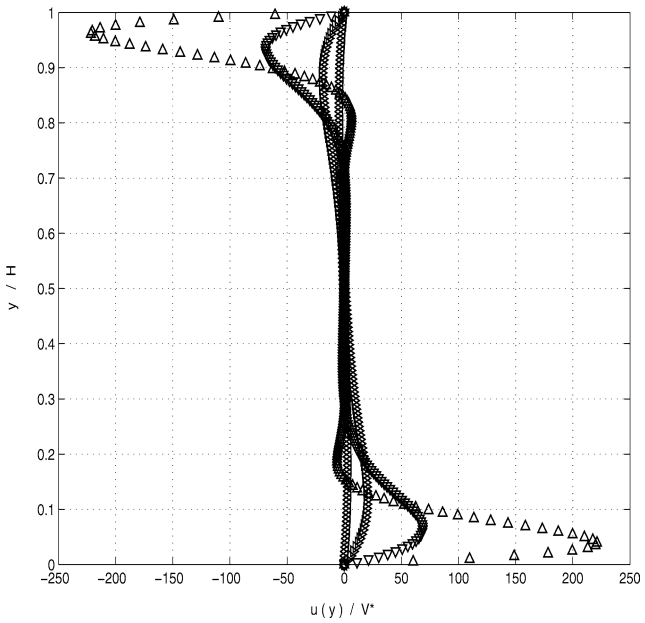

Fig. 4. Normalized vertical velocity at $x/L = 0.5$, $\Delta T = 19.0$, $Pr = 0.71$; $\triangleleft$: $Ra = 10^3$, $\triangleright$: $Ra = 10^4$, $\triangledown$: $Ra = 10^5$, $\triangle$: $Ra = 10^6$.

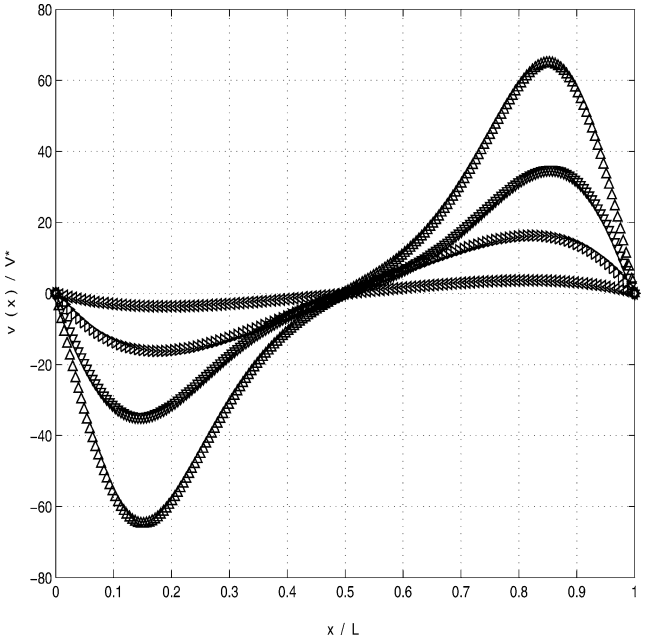

Fig. 5. Normalized horizontal velocity at $y/H = 0.5$, $\Delta T = 19.0$, $Pr = 0.71$; $\triangleleft$: $Ra = 10^3$, $\triangleright$: $Ra = 10^4$, $\triangledown$: $Ra = 10^5$, $\triangle$: $Ra = 10^6$.

two-dimensional flow in a square cavity is considered. At the four walls of the cavity, the velocity is still $(U, V) = (0, 0)$. The horizontal walls (West and East) are insulated, whereas the vertical walls (North and South) are cooled and heated respectively by means of an imposed uniform heat flux (see Fig. 6). In this case, the forcing G representing the buoyancy effects in Eq. (27) is modified as $G_2 = \beta g(T - T_O)$, where T_O is the temperature in the cavity centre. The Rayleigh number based on prescribed heat flux q_y and cavity height or width, is $Ra_2 = \beta g q_y H^4 Pr/\nu^2 k$, where $k = \rho c_v \chi$ is the

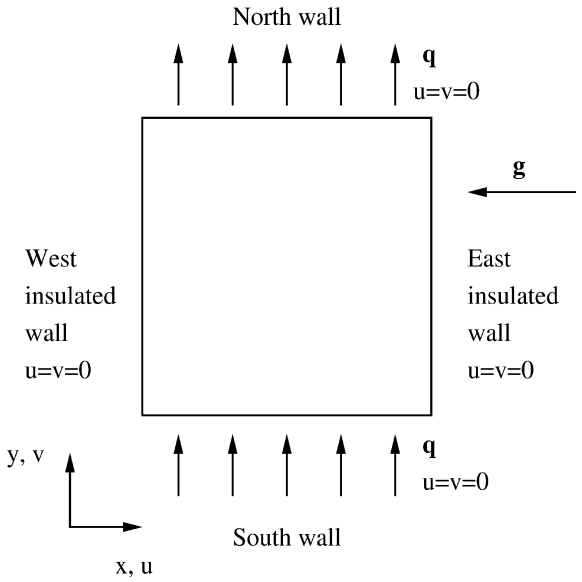

Fig. 6. Imposed heat flux flow configuration.

thermal conductivity. For laminar convection in this flow configuration, still neglecting the viscous heating effects, the reader is referred to the analytical solution given by Kimura and Béjan in [39]. From a theoretical analysis in the context of the boundary layer regime, they found the following relationships between the dimensionless variables into the boundary layer region:

$$\widetilde{T}(\tilde{y}) = -\frac{4}{A} e^{-\frac{A}{4}\tilde{y}} \cos\left(\frac{A}{4}\tilde{y}\right) \tag{39}$$

$$\tilde{u}(\tilde{y}) = -\frac{32}{A^3} e^{-\frac{A}{4}\tilde{y}} \sin\left(\frac{A}{4}\tilde{y}\right) \tag{40}$$

where

$$\tilde{y} = \frac{y}{L\, Ra_2^{-1/5}} \tag{41}$$

$$\widetilde{T} = \frac{T - T_O}{\frac{\chi\nu}{g\beta L^3} Ra_2^{4/5}} \tag{42}$$

$$\tilde{u} = \frac{u}{\frac{\chi}{L} Ra_2^{2/5}} \tag{43}$$

and the constant A is calculated as

$$A^9 = 8192 \frac{L}{H} Ra_2^{1/5} \tag{44}$$

In the core, the temperature $\widetilde{T}_\infty$ and the velocity components $\tilde{u}_\infty$, $\tilde{v}_\infty$ are found

$$\widetilde{T}_\infty = \tilde{x} \frac{A^4}{64}, \qquad \tilde{u}_\infty = 0, \qquad \tilde{v}_\infty = 0 \tag{45}$$

where $\tilde{x} = x/H$. The Nusselt number predicted by their analysis is as follows:

$$\overline{Nu} = 0.340 \left(\frac{L}{H}\right)^{1/9} Ra_2^{2/9} \tag{46}$$

4.1. Boundary conditions

Boundary conditions for the velocity are the same used in Section 3, so the reader is still referred to Appendix A.

At insulated walls (the West wall as an example), the constraints (32) and (34) are applied. In order to impose the uniform heat flux at the vertical walls, the thermal counter-slip approach is applied here along with a non-zero heat flux constraint. This Neumann-type boundary condition appears for the first time in present work, and allows lattice Boltzmann method to handle imposed wall heat fluxes boundary conditions, beyond the usual adiabatic condition of previous schemes.

With reference to the North wall as an example, the constraint on q_y is

$$\sum_i c_{iy}\tilde{g}_i = \frac{\tau_g + 0.5\,\mathrm{d}t}{\tau_g} q_y + 0.5\,\mathrm{d}t \sum_i c_{iy} f_i Z_i + \rho e_N V \tag{47}$$

where e_N denotes the current value (coming from the run) of the North wall thermal energy density, and the viscous dissipation term still appears for generality. The unknown populations $\tilde{g}_{\downarrow}$, $\tilde{g}_{\swarrow}$ and $\tilde{g}_{\searrow}$, as already said, are assumed to be equilibrium distribution functions with a counter-slip thermal energy density e' (see Eq. (29)), and thus become

$$\tilde{g}_{\downarrow,\swarrow,\searrow} = \left[\frac{1}{\frac{1}{3} - 0.5\frac{V}{c} + 0.5\frac{V^2}{c^2}}\right] \times [\text{corresponding form for equilibrium}] \times \left[\left(\sum_{\uparrow,\nearrow,\nwarrow} \tilde{g}_i\right) - \frac{\tau_g + 0.5\,\mathrm{d}t}{\tau_g}\frac{q_y}{c} - \frac{\mathrm{d}t}{2}\sum_N \frac{c_{iy}}{c} Z_i f_i - \rho e_N \frac{V}{c}\right] \tag{48}$$

where explicitly appears a term with the specified heat flux.

4.2. Numerical results

For a comparison with the theoretical solutions given by Kimura and Béjan [39], results for $Ra_2 = 10^5$ and $Ra_2 = 10^6$ with $Pr = 2.0$ and $L/H = 1.0$ are given. A 301×301 grid is used and the relaxation times are chosen $\tau_f = 0.2$ and $\tau_g = 0.05$; the prescribed heating and cooling heat flux is chosen $q_y = 6.702 \times 10^{-5}$. The comparison concerns the dimensionless vertical velocity $u(y)/V^{**}$ and the normalized temperature $[T(y) - T_O]/T^{**}$ at $x/L = 0.5$; the reference variables are $V^{**} = \chi Ra_2^{2/5}/H$ and $T^{**} = \chi\nu Ra_2^{4/5}/\beta g H^3$, respectively. The reference horizontal coordinate is $y^{**} = HRa_2^{-1/5}$. Figs. 7 and 8 refer to $Ra_2 = 10^5$, whereas Figs. 9 and 10 refer to $Ra_2 = 10^6$; all the profiles are plotted for the "hot" half cavity. In Fig. 11 normalized temperature distribution on three vertical planes is presented, as compared with analytical solution, for $Ra_2 = 10^6$.

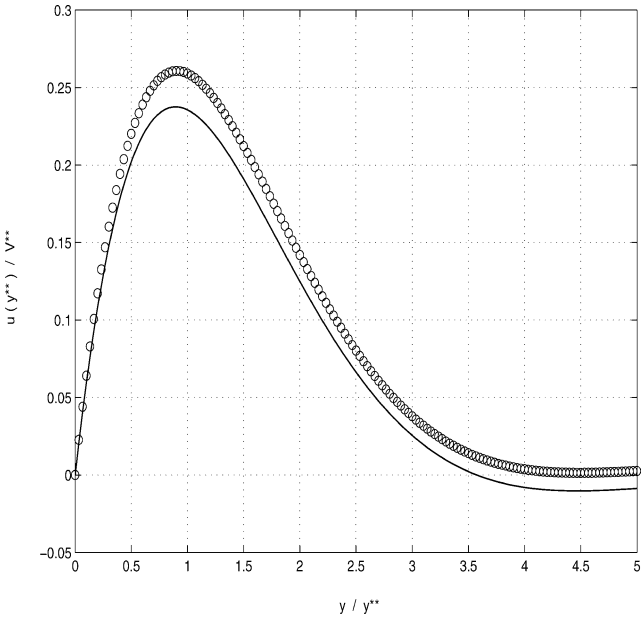

Fig. 7. Hot wall boundary layer: dimensionless vertical velocity profile at $x/L = 0.5$ for $Ra_2 = 10^5$; numerical (circles) versus theoretical (solid line) values.

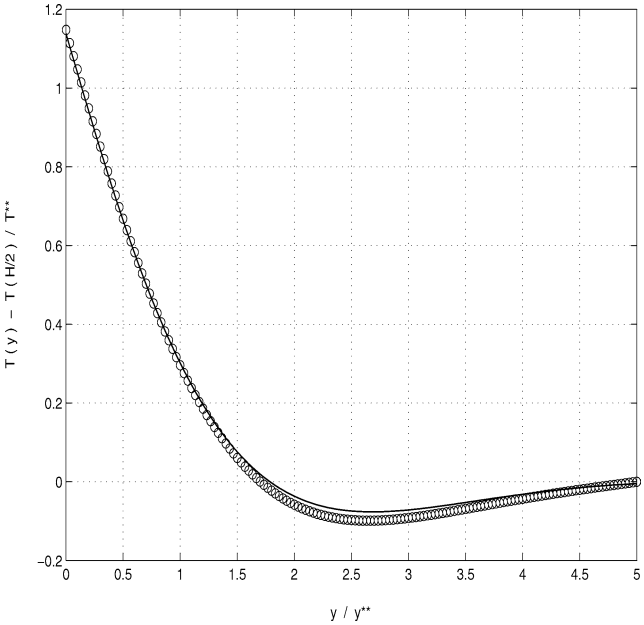

Fig. 8. Hot wall boundary layer: normalized temperature profile at $x/L = 0.5$ for $Ra_2 = 10^5$; numerical (circles) versus theoretical (solid line) values.

Some more remarks are required. The theoretical study was developed under the assumption of boundary layer regime. According to the theoretical boundary layer analysis, temperature and velocity fields close to the heated and cooled vertical walls of the cavity, originate from the direct buoyant contribution by the respective wall itself. The numerical approach takes into account the role played by the opposite wall, whose effects may indeed be non-negligible. Actually, the fluid which flows along the hot (or cold) wall

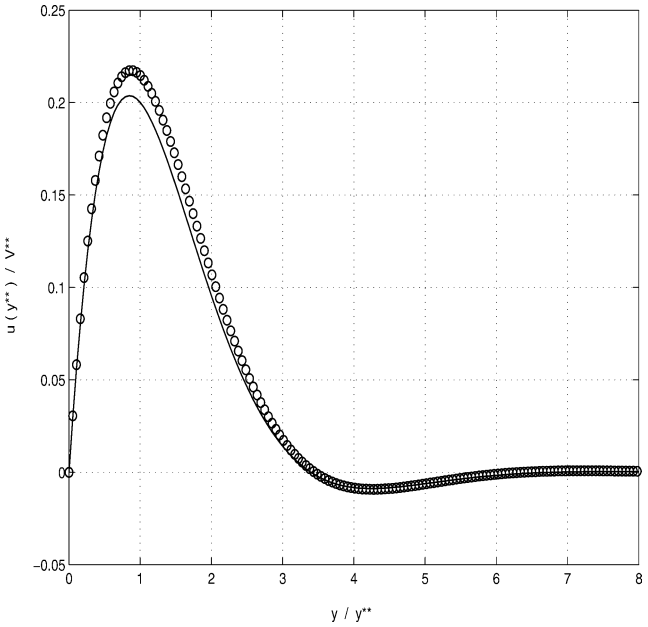

Fig. 9. Hot wall boundary layer: dimensionless vertical velocity profile at $x/L = 0.5$ for $Ra_2 = 10^6$; numerical (circles) versus theoretical (solid line) values.

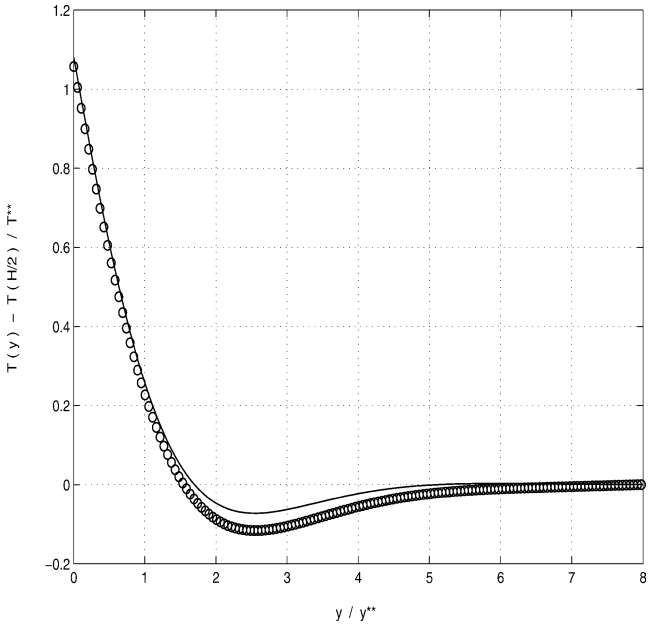

Fig. 10. Hot wall boundary layer: normalized temperature profile at $x/L = 0.5$ for $Ra_2 = 10^6$; numerical (circles) versus theoretical (solid line) values.

of the cavity is previously cooled (or heated) by the opposite wall: a larger amount of heat is transferred from the hot wall to the fluid (or from the fluid to the cold wall), which implies an enhanced buoyancy-induced motion. In addition, one can see from the numerical results the motionless cavity core induced by the opposing effects of the vertical walls, whereas a more extensive boundary layer region is singled out by the theoretical approach. This is more evident in Fig. 7, since the boundary layer thickness increases for lower *Ra*; for higher Rayleigh numbers, a definite separation between the core and the two boundary layer regions is detected, and it makes clear the better agreement between numerical and theoretical results in Fig. 9. The linear thermal stratification is shown in Fig. 11: the near-wall and core temperatures vary linearly with the height, with the exception of the region near the top and bottom walls, where the fluid flows horizontally and the vertical temperature gradient vanishes.

The local Nusselt number and the average value are calculated as

$$Nu_2 = \frac{q_y H}{\Delta T k} \tag{49}$$

$$\overline{Nu}_2 = \frac{1}{L}\int_0^L Nu_2 \,\mathrm{d}x \tag{50}$$

where ΔT is the actual wall-to-wall temperature difference. In Table 3 are reported the local Nusselt number at $x/L = 0.5$ and the average value for both $Ra_2 = 10^5$ and $Ra_2 = 10^6$; the average values are compared with those obtained by means of the theoretical formula (46). It could be noted that the theoretical analysis proposed by Kimura and Béjan [39] refers to $Pr \gg 1.0$ and the numerical results refer

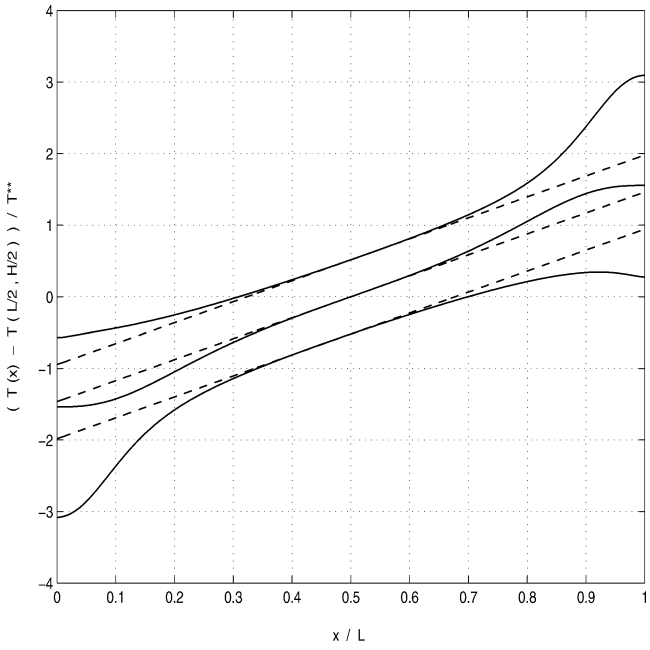

Fig. 11. Normalized temperature distribution for $Ra_2 = 10^6$ at $y/H = 0.0367$ ($y = 0.58108 H Ra_2^{-1/5}$), $y/H = 0.5$ ($y = 7.92384 H Ra_2^{-1/5}$), $y/H = 0.9634$ ($y = 15.26659 H Ra_2^{-1/5}$); numerical (solid lines) versus theoretical (dashed line) values.

to $Pr = 7.0$, falling by 15–20 percent below the theoretical predictions. In this work, errors of 17.2 and 12 percent for $Ra_2 = 10^5$ and $Ra_2 = 10^6$, respectively are found.

Table 3
Natural convection in a square cavity with uniform heat flux from vertical walls: Nusselt number (Nu_2) for different Rayleigh number (Ra_2) and $Pr = 2.0$

Ra	$\overline{Nu}$	$Nu_{x/L=0.5}$	$\overline{Nu}$ theoretical
10^5	3.6374	4.3449	4.3909
10^6	6.4423	7.4856	7.3244

5. Conclusions

A thermal lattice Boltzmann BGK model with doubled populations has been discussed. With respect to previous LB methods, it enhances the numerical stability and is able to include the viscous heating effects. A new thermal boundary condition for this scheme has been proposed. It can simulate explicitly either imposed wall temperature (Dirichlet-type constraint) or imposed wall heat fluxes (Neumann-type constraint), beyond the adiabatic condition of previous schemes. These significant improvements, in the context of the kinetic schemes, can be added to the advantages specific to these methods, and primarily to lattice Boltzmann methods. They include fully parallel algorithms and easy implementation of interfacial dynamics and complex boundaries, as in single and multi-phase flow in porous media. In addition, no Poisson equation must be resolved and irregular boundary conditions are easy to handle. It makes the lattice Boltzmann methods competitive tools, with respect to the usual theoretical approaches and to the standard numerical techniques, for the simulation of complex hydrodynamic phenomena, from fully developed turbulence to phase transitions to granular flows.

Application to different cases of natural convection in a cavity has been carried out. The study shows that this method provides reliable results over a wide range of physical parameters. Thus it can become an effective and alternative tool, as well as the athermal counterpart, for successful simulation of many types of heat transfer and fluid flow processes, especially for all situations where complex phenomena take places.

Appendix A

In order to describe the procedure proposed by Zou and He [36] to impose the velocity boundary conditions, the reference as an example is to the West wall, where the unknown populations coming from the external nodes are $\tilde{f}_{\rightarrow}$, $\tilde{f}_{\nearrow}$, $\tilde{f}_{\searrow}$, and the arrows are self-explanatory for the streaming directions. The wall speed $(U, V) = (0, 0)$ has been imposed by means of the constraints:

$$\sum_i \tilde{f}_i = \rho_W, \qquad \sum_i \tilde{f}_i c_{ix} = \rho_W U - \frac{\mathrm{d}t}{2} F_b$$
$$\sum_i \tilde{f}_i c_{iy} = \rho_W V \tag{A.1}$$

plus a "bounce-back" condition on the non-equilibrium part of the particle distribution perpendicular to the boundary:

$$\tilde{f}_{\rightarrow} - f^e_{\rightarrow} = \tilde{f}_{\leftarrow} - f^e_{\leftarrow} \tag{A.2}$$

These yield the wall density as a function of the known populations (those inside the computational domain) and of the wall speed $(U, V) = (0, 0)$:

$$\rho_W = \left[\left(\sum_{\text{known } \tilde{f}_i} \tilde{f}_i\right) + \tilde{f}_{\leftarrow} + \tilde{f}_{\swarrow} + \tilde{f}_{\nwarrow}\right] \times \frac{1}{1 - \frac{U}{c} + 0.5\,\mathrm{d}t\frac{G}{c}} \tag{A.3}$$

It follows that

$$\tilde{f}_{\rightarrow} = \tilde{f}_{\leftarrow} + \frac{2}{3}\rho_W \frac{U}{c} \tag{A.4}$$

$$\tilde{f}_{\nearrow} = \tilde{f}_{\swarrow} + \frac{\tilde{f}_{\downarrow} - \tilde{f}_{\uparrow}}{2} + \frac{1}{6}\rho_W \frac{U}{c} + \frac{1}{2}\rho_W \frac{V}{c} - 0.25\,\mathrm{d}t\frac{F_b}{c} \tag{A.5}$$

$$\tilde{f}_{\searrow} = \tilde{f}_{\nwarrow} - \frac{\tilde{f}_{\downarrow} - \tilde{f}_{\uparrow}}{2} + \frac{1}{6}\rho_W \frac{U}{c} - \frac{1}{2}\rho_W \frac{V}{c} - 0.25\,\mathrm{d}t\frac{F_b}{c} \tag{A.6}$$

The constrains for a corner node (the North–West corner as an example) are the same in Eq. (A.1) plus the two non-equilibrium bounce back conditions on the particle distributions perpendicular to the boundaries

$$\tilde{f}_{\rightarrow} - f^e_{\rightarrow} = \tilde{f}_{\leftarrow} - f^e_{\leftarrow}$$
$$\tilde{f}_{\downarrow} - f^e_{\downarrow} = \tilde{f}_{\uparrow} - f^e_{\uparrow} \tag{A.7}$$

The five unknown distributions incoming at the corner are thus found as:

$$\tilde{f}_{\rightarrow} = \tilde{f}_{\leftarrow} + \frac{2}{3}\rho_{NW} \frac{U}{c} \tag{A.8}$$

$$\tilde{f}_{\downarrow} = \tilde{f}_{\uparrow} - \frac{2}{3}\rho_{NW} \frac{V}{c} \tag{A.9}$$

$$\tilde{f}_{\nearrow} = \frac{\rho_{NW} - \tilde{f}_0}{2} - \frac{1}{3}\rho_{NW} \frac{U}{c} + \frac{1}{2}\rho_{NW} \frac{V}{c} - \left(\tilde{f}_{\leftarrow} + \tilde{f}_{\uparrow} + \tilde{f}_{\nwarrow}\right) \tag{A.10}$$

$$\tilde{f}_{\swarrow} = \frac{\rho_{NW} - \tilde{f}_0}{2} - \frac{1}{2}\rho_{NW} \frac{U}{c} + \frac{1}{3}\rho_{NW} \frac{V}{c} - \left(\tilde{f}_{\leftarrow} + \tilde{f}_{\uparrow} + \tilde{f}_{\nwarrow}\right) + 0.25\,\mathrm{d}t\frac{F_b}{c} \tag{A.11}$$

$$\tilde{f}_{\searrow} = \tilde{f}_{\nwarrow} + \frac{1}{6}\rho_{NW} \frac{U}{c} - \frac{1}{6}\rho_{NW} \frac{V}{c} - 0.25\,\mathrm{d}t\frac{F_b}{c} \tag{A.12}$$

where ρ_{NW} can be taken equal to the density value of the nearest neighbour node.

References

[1] J. Higuera, S. Succi, R. Benzi, Lattice gas-dynamics with enhanced collisions, Europhys. Lett. 9 (4) (1989) 345–349.

[2] R. Benzi, S. Succi, M. Vergassola, The lattice Boltzmann equation: theory and applications, Phys. Reports 222 (3) (1992) 145–197.

[3] F. Alexander, S. Chen, J. Sterling, Lattice Boltzmann thermohydrodynamics, Phys. Rev. E 47 (4) (1993) 2249–2252.

[4] S. Chen, G. Doolen, Lattice Boltzmann method for fluid flows, Annual Rev. Fluid Mech. 30 (1998) 329–364.

[5] S. Succi, The Lattice Boltzmann Equation—For Fluid Dynamics and Beyond, Oxford Univ. Press, Oxford, 2001.

[6] X. Nie, G. Doolen, S. Chen, Lattice–Boltzmann simulations of fluid flows in MEMS, J. Statist. Phys. 107 (1) (2002) 279–289.

[7] C. Lim, C. Shu, X. Niu, Y. Chew, Application of lattice Boltzmann method to simulate microchannel flows, Phys. Fluids 14 (7) (2002) 2299–2308.

[8] H. Nguyen, B. Chopard, S. Stoll, Lattice Boltzmann method to study hydrodynamic properties of 2D fractal aggregates, in: P. Sloot, D. Abramson, A. Bogdanov, J. Dongarra, A. Zomaya, Y. Gorbachev (Eds.), Proceedings of International Conference of Computational Science, ICCS 2003, Springer, Berlin, 2003, pp. 947–956.

[9] A. Hoekstra, J. van't Hoff, A. Artoli, P. Sloot, Lattice BGK simulations of unsteady flow in a 2D elastic tube, in: P. Sloot, D. Abramson, A. Bogdanov, J. Dongarra, A. Zomaya, Y. Gorbachev (Eds.), Proceedings of International Conference of Computational Science, ICCS 2003, Springer, Berlin, 2003, pp. 997–1006.

[10] P. Facin, P. Philippi, L. dos Santos, A three-parameter non-linear lattice–Boltzmann model for ideal miscible fluids, in: P. Sloot, D. Abramson, A. Bogdanov, J. Dongarra, A. Zomaya, Y. Gorbachev (Eds.), Proceedings of International Conference of Computational Science, ICCS 2003, Springer, Berlin, 2003, pp. 1007–1014.

[11] T. Inamuro, T. Ogata, F. Ogino, Lattice Boltzmann simulation of bubble flows, in: P. Sloot, D. Abramson, A. Bogdanov, J. Dongarra, A. Zomaya, Y. Gorbachev (Eds.), Proceedings of International Conference of Computational Science, ICCS 2003, Springer, Berlin, 2003, pp. 1015–1023.

[12] A. Dupuis, A. Briant, C. Pooley, J. Yeomans, Droplet spreading on heterogeneous surfaces using a three-dimensional lattice Boltzmann model, in: P. Sloot, D. Abramson, A. Bogdanov, J. Dongarra, A. Zomaya, Y. Gorbachev (Eds.), Proceedings of International Conference of Computational Science, ICCS 2003, Springer, Berlin, 2003, pp. 1024–1033.

[13] Y. Chen, H. Ohashi, M. Akiyama, Thermal lattice Bhatnagar–Gross–Krook model without non-linear deviations in macrodynamic equations, Phys. Rev. E 50 (1994) 2776–2783.

[14] Y. Chen, H. Ohashi, M. Akiyama, Prandtl number of lattice Bhatnagar–Gross–Krook fluid, Phys. Fluids 7 (1995) 2280–2282.

[15] G. Mc Namara, A. Garcia, B. Alder, Stabilization of thermal lattice Boltzmann models, J. Statist. Phys. 81 (1/2) (1995) 395–408.

[16] H. Chen, H-theorem and generalized semi-detailed balance condition for lattice gas system, J. Statist. Phys. 81 (1/2) (1995) 347–360.

[17] G. Vahala, P. Pavlo, L. Vahala, N. Martys, Thermal lattice Boltzmann models for compressible flows, Internat. J. Modern Phys. C 9 (8) (1998) 1247–1261.

[18] I.V. Karlin, A. Ferrante, H.C. Öttinger, Perfect entropy functions of the lattice Boltzmann method, Europhys. Lett. 47 (1999) 182–188.

[19] L.S. Luo, Some recent results on discrete velocity models and ramifications for lattice Boltzmann equation, Comput. Phys. Comm. 129 (1/3) (1999) 63–74.

[20] S. Succi, I. Karlin, H. Chen, Colloquium: Role of the H theorem in Lattice Boltzmann hydrodynamic simulations, Rev. Mod. Phys. 74 (4) (2002) 1203–1220.

[21] P. Lallemand, L.S. Luo, Hybrid finite-difference thermal lattice Boltzmann equation, Internat. J. Modern Phys. B 17 (1/2) (2003) 41–47.

[22] X. He, S. Chen, G. Doolen, A novel thermal model for the lattice Boltzmann method in incompressible limit, J. Comput. Phys. 146 (1998) 282–300.

[23] A. D'Orazio, S. Succi, Boundary conditions for thermal lattice Boltzmann simulations, in: P. Sloot, D. Abramson, A. Bogdanov, J. Dongarra, A. Zomaya, Y. Gorbachev (Eds.), Proceedings of International Conference of Computational Science, ICCS 2003, Springer, Berlin, 2003, pp. 1024–1033.

[24] A. D'Orazio, S. Succi, A. Arrighetti, Lattice Boltzmann simulation of open flows with heat transfer, Phys. Fluids 15 (9) (2003) 2778–2781.

[25] A. Janssen, M. Henkes, J. Hoogendorn, Transition to time-periodicity of a natural convection flow in a 3D differentially heated cavity, Internat. J. Heat Mass Transfer 30 (1987) 1645–1654.

[26] S. Xin, P. Le Quere, Direct numerical simulations of two-dimensional chaotic natural convection in a differentially heated cavity of aspect ratio 4, J. Fluid Mech. 304 (1995) 87–118.

[27] M. Versteegh, M. Nieuwstadt, A direct numerical simulation of natural convection between two infinite vertical differentially heated walls—scaling laws and wall functions, Internat. J. Heat Mass Transfer 42 (1999) 3673–3693.

[28] S. Dol, K. Hanjalic, Computational study of turbulent natural convection in a side-heated near-cubic enclosures at high Rayleigh number, Internat. J. Heat Mass Transfer 44 (2001) 2323–2344.

[29] Q. Wang, H. Yoo, Y. Jaluria, Convection in a horizontal rectangular duct under constant and variable property formulations, Internat. J. Heat Mass Transfer 46 (2003) 297–310.

[30] M. Corcione, Effects of the thermal boundary conditions at the sidewalls upon natural convection in rectangular enclosures heated from below and cooled from above, Internat. J. Thermal Sci. 42 (2) (2003) 199–208.

[31] Y. Qian, D. d'Humiéres, P. Lallemand, Lattice BGK models for Navier–Stokes equation, Europhys. Lett. 17 (6) (1992) 479–484.

[32] X. He, L. Luo, A priori derivation of the lattice Boltzmann equation, Phys. Rev. E 55 (6) (1997) 6333–6336.

[33] M. Hortmann, M. Perić, G. Scheuerer, Finite volume multigrid prediction of laminar natural convection: bench-mark solutions, Internat. J. Numer. Methods Fluids 11 (1990) 189–207.

[34] G. De Vahl Davis, Natural convection of air in a square cavity: a bench mark numerical solution, Internat. J. Numer. Methods Fluids 3 (1983) 249–264.

[35] G. Barakos, E. Mitsoulis, D. Assimacopoulos, Natural convection flow in a square cavity revisited: laminar and turbulent models with wall functions, Internat. J. Numer. Methods Fluids 18 (1994) 695–719.

[36] Q. Zou, X. He, On pressure and velocity boundary conditions for the lattice Boltzmann BGK model, Phys. Fluids 9 (6) (1997) 1591–1598.

[37] T. Inamuro, M. Yoshino, F. Ogino, A non-slip boundary condition for lattice Boltzmann simulations, Phys. Fluids 7 (12) (1995) 2928–2930.

[38] X. He, Q. Zou, L.S. Luo, M. Dembo, Analytic solutions and analysis on non-slip boundary condition for the lattice Boltzmann BGK model, J. Statist. Phys. 87 (1/2) (1997) 115–136.

[39] S. Kimura, A. Béjan, The boundary layer natural convection regime in a rectangular cavity with uniform heat flux from the side, ASME J. Heat Transfer 106 (1984) 98–103.